Simulation and modeling of reacting particles in turbulent nonpremixed combustion

By N. S. A. Smith[1], G. R. Ruetsch, J. Oefelein, AND J. H. Ferziger

A conditional moment closure model is proposed for reacting particles in turbulent nonpremixed combustion. The new model for particles differs significantly from the traditional uniform diffusivity gas-phase conditional moment closure model. The new features of the model and its effectiveness are examined against direct numerical simulation data for soot-like and droplet-like particles in turbulent nonpremixed combustion. The influence of differing particle sizes and types on the effectiveness of the model closure is examined in detail.

1. Introduction

Condensed-phase particles are frequently present in turbulent combustion systems and can have a profound influence on the thermochemical nature of their surroundings. Fuel droplets and soot particles are two examples of important condensed phase species in combustion. The evaporation of the former largely determines the distribution of the combustible gaseous fuel/air mixture, while the presence of the latter impacts strongly on the degree of radiant heat transfer from the system. It is thus desirable to be able to predict the mean behavior of these particles, in a turbulent combusting environment, in response to their local thermochemical conditions.

A number of difficulties surround the modeling of the mean rate of particle reactions in turbulent combustion. Perhaps the most significant difficulty is associated with determining the mean influence of carrier fluid properties such as temperature and chemical species concentrations upon the particle population. Wherever the local properties of the carrier fluid fluctuate due to turbulence, the variations can couple with the non-linear particle reactions to preclude first order closure of the mean rates with mean properties. This type of closure problem is the same as that encountered in modeling the mean rate of purely gas phase chemical reactions using conventional averaging techniques.

The Conditional Moment Closure (CMC) method (see Klimenko 1990, Bilger 1993) for modeling turbulent gas phase nonpremixed combustion makes use of averages which are conditional upon the local value of a conserved scalar (mixture fraction), which is indicative of the state of mixing between fuel and air masses. Conditional averaging upon mixture fraction captures much of the turbulence-induced fluctuations, and a first order conditionally averaged closure is often possible. The success of the CMC model in predicting gas phase combustion makes it of some interest in modeling particle reactions in turbulent flow.

1 Aeronautical & Maritime Research Laboratory, DSTO, Australia

The purpose of this study was to simulate the dynamics of reactive particle mass and motion in a turbulent combusting environment in an attempt to model the observed mean thermochemical behavior of the reacting particles using a derivative of the CMC method. In this report, the simulation and modeling of pseudo-soot and pseudo-droplet particles are described. The former type of particles were smaller than the latter, and they were subject to relatively strong processes of growth and consumption. These processes were meant to represent soot surface growth and oxidation. The pseudo-droplet particles were subject to an evaporative process only. In both the simulations and modeling, particle-particle interactions were disallowed, thus rendering the results of this study valid only for low particle mass loadings of the gas phase.

2. Simulation conditions

Direct numerical simulations were conducted using a pseudo-spectral solution technique for forced isotropic turbulent flow on a 32-cubed grid. The flow was incompressible in nature, but a passive scalar (mixture fraction) field was used in conjunction with an equilibrium temperature profile in passive scalar space to determine a false temperature map throughout the domain. This false temperature was computed for the purpose of determining instantaneous particle reaction rates at every step. The passive scalar field was forced at large scales through the interaction of turbulent motions with an imposed mean scalar gradient in the x direction in the same manner as the simulations of Overholt and Pope (1996). Cubic spline tensor-products as described by Yeung and Pope (1988, 1989) were employed to determine local fluid velocities and temperatures at all particle locations. Particle properties were advanced in time using a fourth-order Adams-Bashforth timestepping routine.

The following Lagrangian equation for particle motion was solved,

$$\frac{dv_i}{dt} = \frac{\alpha^*}{\tau_k} \left(m^*\right)^{-2/3} \left(u_i(\underline{x}) - v_i\right) \quad , \tag{1}$$

where v_i denotes the particle velocity, $u_i(\underline{x})$ denotes the local fluid velocity at the particle location, m^* is the nondimensional particle mass, τ_k is the Kolmogorov timescale, and α^* is the nondimensional characteristic particle rate given by,

$$\alpha^* = 18 \left(\frac{\rho_f}{\rho_p}\right) \left(\frac{\text{Ł}_k}{d}\right)^2 \quad . \tag{2}$$

In the above, Ł$_k$ is the Kolmogorov length scale, d is the reference particle diameter, ρ_p is the particle material density, and ρ_f is the fluid density.

The Stokes drag expression above (Eq. 1) strictly applies only in the limit of a purely laminar flow around the particle. This assumption is valid for the smaller soot particles but is not as well justified for the droplets. Empirical corrections for changes in particle drag with higher slip Reynolds numbers are available but have not been applied in the simulations reported here.

For droplets, the rate of change of the mass of any particle was given by

$$\frac{dm^*}{dt} = -\frac{2}{3}\frac{\beta}{\tau_k}\left(m^*\right)^{1/3}\ln(1+T^*) \quad , \tag{3}$$

where β is a generic rate coefficient, nominally equal to α^* for inertial particles, and T^* is a nondimensional temperature equivalent to the local *Spalding transfer number*. The value of the temperature varied from zero in non-reactive regions of passive scalar space to a peak value of 3.4 at stoichiometric conditions. The peak value corresponds to the transfer number for kerosene droplets evaporating within enveloping flames (see Kuo 1986).

The rate of change of mass for any given soot particle was given by

$$\frac{dm^*}{dt} = \frac{\beta}{\tau_k}\left(m^*\right)^{1/3}\left(f_{gr} - f_{co}\left(m^*\right)^{1/3}\right) \quad , \tag{4}$$

where β is a rate coefficient not directly related to α^*, and f_{gr} and f_{co} are normalized functions of local mixture fraction (and thus an inferred reactive gas phase composition) which mimic surface growth and consumption respectively. The growth and consumption reactions were designed to embody the basic features of the soot processes they represent, but with one notable difference. Namely, the reaction rate profiles were defined so as to be symmetric in mixture fraction space about the mean mixture fraction. Particle surface growth was strongest at the mean mixture fraction, and particle consumption was strongest somewhat to the lean and rich sides of the mean mixture fraction. This symmetry of thermochemical properties about the mean mixture fraction allowed conditional statistics on either side of the mean to be combined to increase statistical significance in each half-plane of mixture fraction space.

The reference particle rates (α^*, β) differed between simulations to reflect different sizes and reactivity of the particles, while flow and mixing conditions were the same for all cases. The details of the simulation cases studied are given in Table I. Some inertial particle simulations were repeated with inertia-less particles (denoted by i-suffixed case designations in Table I) to ascertain the influence of particle slip velocity on the reactive particle statistics.

Table I. Parameters and durations for the reactive particle simulations.

Case	Type	α^*	β	τ_{sim}/τ_{eddy}	τ_{sim}/τ_{pop}
d1	droplet	0.014	0.014	193	34.7
d1i	droplet	∞	0.014	96.1	15.0
s1	soot	0.7	2.8	3.5	0.46
s2	soot	0.7	0.7	104	23.1
s2i	soot	∞	0.7	104	23.1

In the table, the ratios of the duration (τ_{sim}) of each case to both the large eddy turnover time (τ_{eddy}) and the mean time for total particle population change through injection (τ_{pop}) are given. Owing to explicit method time step limitations, the cases with longer characteristic timescales such as the droplet and less-reactive soot cases were less expensive to compute. These cases, therefore, could be continued for a larger number of eddy-turnover times for a given amount of real time.

In each case, 8192 particles were maintained in the domain at a constant mean number density by continuous injection. Particle simulations commenced only after the forcing had produced a statistically stationary flow field over a period of many hundreds of eddy turnover times. The simulations were conducted at a Taylor Reynolds number of ~ 24 with a value of approximately 0.22 for the ratio of integral length scale to domain width and 2.4 for the product of Kolmogorov lengthscale and maximum wavenumber in the simulation.

The actual size of the soot particles used in the *inertial* simulations of this study were at the upper limit of realistic soot particles. In a sense, these simulation cases embody a *worst case scenario* for modeling soot. In practical applications, the bulk of soot particles are much smaller and follow the flow field much more closely. These smaller reacting particles were better simulated using an inertia-less particle tracking method in conjunction with the direct numerical simulations of turbulence.

2.1 Particle injection

The imposed mean scalar gradient in the x direction of the simulation domain required that special consideration be given to particles which crossed the domain boundaries in this direction. In the other directions, all properties were periodic and particles were simply returned to the domain by a periodic mapping. The same mapping was not applied in the x direction as that would allow particles to transfer between very lean and very rich mixture conditions in crossing the domain boundary.

Instead, any particle which crossed an x boundary was deemed to have left the domain permanently, and was replaced via a periodic mapping by a fresh particle with a velocity equal to the departing particle and mass equal to the injection mass. This type of fresh particle injection allowed a statistically stationary particle state to be reached as a balance between the processes of particle reaction, and transport to and from the injection boundaries occurs.

Injection across the two x-bounding planes was characterized by a relatively weak influence on conditional mean particle statistics at very rich and lean mixture fractions. The source terms for the conditional mean and variance equations for particle mass fraction which result from these injection schemes are described in Section 3.2.

2.2 Mixing and reaction statistics

Statistical data based on particle mass fractions were measured from the simulations for comparison with model predictions. These data were recorded only after the statistical stationarity of the particle ensemble had been established by monitoring initial transients in the data.

As each particle, on average, occupied four grid cells to the exclusion of other particles, it was not possible to determine meaningful spatial gradients in particle properties within the carrier fluid. It was possible, however, to derive conditional statistical information from the data by binning particles in mixture fraction space according to their local value of mixture fraction. The particle density in each bin allowed gradients of conditional quantities in mixture fraction space to be determined for comparison with modeled terms.

Mixing statistics such as conditional mean scalar dissipation rate, conditional mean scalar diffusion rate, and the mixture fraction probability density function (PDF) were determined from the statistically stationary simulation data.

The mean scalar dissipation rate ($N_\eta \equiv \left\langle \mathcal{D}(\nabla\xi)^2 \mid \xi(\underline{x},t) = \eta \right\rangle$), conditional upon the value (η) of the local instantaneous value of mixture fraction (ξ), was found to be independent of mixture fraction as reported by Overholt and Pope (1996) and Pope and Ching (1993). Thus the significant simplification,

$$N_\eta = \langle N \mid \eta \rangle = \langle N \rangle \quad , \tag{5}$$

was employed in the modeling described below.

The mixture fraction PDF (P_η) for the whole domain was found to agree closely with a superposition of Gaussian PDFs with equal variance, but with mean values varying with position in the x direction according to the imposed mean mixture fraction gradient. Given values of mean mixture fraction on the x boundaries of ξ_0 and ξ_1 and a spatially uniform mixture fraction variance σ^2, the mixture fraction PDF can be written as,

$$P_\eta = \frac{\sigma}{\xi_0 - \xi_1}\left(\phi\left(\frac{\eta-\xi_1}{\sigma}\right) - \phi\left(\frac{\eta-\xi_0}{\sigma}\right)\right) \quad , \tag{6}$$

where $\phi(\ldots)$ is the integral of the Gaussian distribution between the given argument and infinity.

The conditional mean scalar diffusion rate ($M_\eta \equiv \left\langle \mathcal{D}\nabla^2\xi \mid \xi(\underline{x},t) = \eta \right\rangle$) is yielded by,

$$\frac{\partial}{\partial\eta}\left(P_\eta M_\eta\right) = \frac{\partial^2}{\partial\eta^2}\left(P_\eta N_\eta\right) \quad , \tag{7}$$

which holds for homogeneous mixing conditions. The simplification afforded by Eq. 5, thus gives M_η as,

$$M_\eta = \frac{\langle N \rangle}{P_\eta}\frac{\partial P_\eta}{\partial\eta} \quad . \tag{8}$$

The conditional diffusion profile given by the equation above was found to closely agree with the simulation data.

The forms of the mixture fraction PDF and conditional diffusion rate profiles given by the above equations are plotted in Fig. 1. The mixture fraction PDF is somewhat broadened around the peak compared to any single Gaussian profile with the same mean and variance. As a result, the conditional diffusion rate profile has

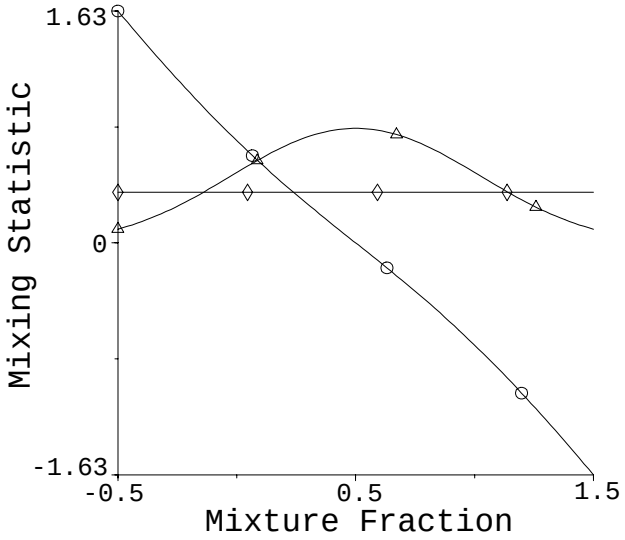

FIGURE 1. Profiles for mixture fraction PDF (△), conditional mean scalar dissipation rate (◇), and conditional mean diffusion rate (○) expected and observed in simulation data.

a mean slope which is about 35% shallower than that of the purely linear profile which results from a single Gaussian PDF with an equivalent mean and variance, and equivalent conditional mean dissipation rate.

All of the simulations exhibited profiles of the nature depicted in the figure since they all shared exactly the same mixing characteristics. The spatially uniform value of variance of mixture fraction was equal to ~ 0.34 in each case, with mean mixture fractions on the x boundaries of zero and unity and an overall domain-averaged mean mixture fraction of one half.

Notice from Fig. 1 that the quantity ξ, referred to here as *mixture fraction*, is normalized to have a unit value on the rich boundary of the domain and zero value on the lean boundary, but this *does not* denote pure fuel and oxidizer states. It is possible, and indeed required in the current simulation configuration, to have values of ξ which are greater than unity and less than zero. Pure fuel and oxidizer states can be considered to exist only in the limits of $\xi \rightarrow \pm\infty$.

3. Modeling method

Application of the CMC model for gas phase turbulent combustion to the modeling of condensed-phase fields requires some consideration of the differences in behavior between the two phases. Firstly, it was assumed that the particles were, in the mean, small enough to follow the smallest scales of motion. This was true in the inertia-less particle simulations, but was somewhat less justified for the inertial (particularly droplet) simulations.

Secondly, it is clear that the particle phase does not diffuse appreciably on a molecular level, and thus the particle phase and the gas phase-based mixture fraction are transported in a completely different manner at this level. The effect of this differential diffusion must, therefore, be incorporated into the CMC model.

Further, at the smallest scales a distinct difference between the distribution of gaseous species and condensed phase species is expected (see Klimenko 1990). Significant local structure can exist in the particle field at scales where gas phase fields have been completely smeared by molecular diffusion. The existence of such local structure implies that instantaneous local deviations of particle mass fractions from means, conditional upon mixture fraction, can be large.

In the present study, particle effects upon the gas phase were neglected, leaving the effect of gas phase fluctuations on particle evolution to be examined in isolation. In reality, however, reciprocal interactions between gaseous and condensed-phase species is likely to be very important. In the case of droplet evaporation, it is the addition of vaporized fuel to the continuous phase which largely determines the way in which combustion proceeds. In the case of soot particles, the removal of sensible enthalpy from the continuous phase occurs as a result of proximity to soot, which can strongly effect localized combustion dynamics. In both of these instances, large conditional variance in particle properties could lead to similarly elevated levels of conditional variance in *sympathetic* gas phase species and thereby increase the difficulty of the chemical closure problem in the gas phase. This increase in conditional variance for gas phase species can be viewed as arising from the different gas phase behavior, at the same mixture fraction, which will result depending on whether a parcel of gas is adjacent to a particle or not.

It is for this reason that it is important to be able to predict the level of conditional variance of particle mass fraction. The CMC model proposed in this study made use of a particle-specific differential diffusion variant of the second-order conditional moment closure proposed by Li and Bilger (1996).

3.1 Model derivation

In the following, a CMC model for particle reactions in turbulent nonpremixed combustion is derived for general flow and mixing conditions. The spatial and temporal simplifications afforded by the simulation conditions of the present study are introduced in Section 3.2.

The local instantaneous equations for mixture fraction and a particle mass fraction continuum form the basis for the derivation of the model. The equation for mixture fraction ξ can be written as,

$$\frac{\partial \xi}{\partial t} + u_i \frac{\partial \xi}{\partial x_i} - \mathcal{D} \frac{\partial^2 \xi}{\partial x_j^2} = 0 \quad , \tag{9}$$

where the flow field is assumed to be incompressible, u_i is the component of carrier fluid velocity in the i-th direction, and $\mathcal{D}$ is the diffusivity of mixture fraction under a Fickian transport assumption.

The equation for local instantaneous mass fraction of the particle continuum is given by,

$$\frac{\partial Y}{\partial t} + v_i \frac{\partial Y}{\partial x_i} - \mathcal{D}_y \frac{\partial^2 Y}{\partial x_j^2} = \dot{\omega} \quad , \tag{10}$$

where $\dot{\omega}$ is the local reaction rate of the particle continuum, $\mathcal{D}_y$ is the effective diffusivity of this continuum, and v_i is the velocity component in the i-th direction of the field of particles. The particle diffusivity $\mathcal{D}_y$ is expected to be very much smaller than the mixture fraction diffusivity; however, the term is retained in the derivation for completeness. Multiplying Eq. 10 by the particle mass fraction yields,

$$\frac{\partial Y^2}{\partial t} + v_i \frac{\partial Y^2}{\partial x_i} - 2\mathcal{D}_y Y \frac{\partial^2 Y}{\partial x_j^2} = 2Y\dot{\omega} \quad , \tag{11}$$

which is used in the derivation of the equation for conditional variance of particle mass fraction.

The *fine-grain* probability density function (see Pope 1985) for mixture fraction is defined as,

$$\psi\left(\underline{x}, t, \eta\right) \equiv \delta\left(\xi\left(\underline{x}, t\right) - \eta\right) \quad , \tag{12}$$

and has an expectation over the statistical ensemble equal to the mixture fraction PDF (P_η) as given by,

$$P_\eta\left(\underline{x}, t, \eta\right) = \langle\psi\rangle \quad . \tag{13}$$

The local instantaneous equation for the *fine-grained* PDF can be derived from the differential properties of ψ and Eq. 9 so that,

$$\frac{\partial \psi}{\partial t} + \frac{\partial}{\partial x_i}\left(u_i \psi\right) + \frac{\partial}{\partial \eta}\left(\mathcal{D}\psi\nabla^2\xi\right) = 0 \quad . \tag{14}$$

Klimenko and Bilger (1998) derived a conditional mean equation for the differential diffusion of gaseous species in turbulent combustion through the combination of Eqs. 11 and 14 given above. Their methodology is largely followed here except that a conditional variance equation is also derived and some significant differences in closure assumptions are made in the final stages. In the section immediately following, derivation of the equation for the product of the square of particle mass fraction and the fine grain PDF is described as a prerequisite to the derivation of the conditional variance equation for particle mass fraction. The derivation of the corresponding equation for conditional mean mass fraction is analogous except where noted otherwise.

3.1.1. Derivation of ψY^2 equation

The derivation proceeds by adding Eq. 11, multiplied by ψ, to Eq. 14, multiplied by Y^2. The resultant equation is given by,

$$\frac{\partial}{\partial t}\left(\psi Y^2\right) + \frac{\partial}{\partial x_i}\left(u_i \psi Y^2\right) = \left(u_i - v_i\right)\psi \frac{\partial Y^2}{\partial x_i} + 2\psi Y\dot{\omega} + A_y - A_\xi \quad , \tag{15}$$

where

$$A_y = 2\mathcal{D}_y \psi Y \frac{\partial^2 Y}{\partial x_j^2} \quad , \quad A_\xi = Y^2 \frac{\partial}{\partial \eta}\left(\psi\mathcal{D}\nabla^2\xi\right),$$

are convenient groupings of the $\mathcal{D}$ and $\mathcal{D}_y$ diffusive terms. The mixture fraction diffusivity term, first expanded by using the inhomogeneous-flow form of Eq. 7, is

$$A_\xi = Y^2 \left(\frac{\partial^2}{\partial \eta^2} \left(\psi \mathcal{D} \left(\nabla \xi \right)^2 \right) - \mathcal{D} \frac{\partial^2}{\partial x_j^2} \left(\psi \right) \right) \quad . \tag{16}$$

The latter right-hand side term appearing in Eq. 16 also appears in the full expansion of $\mathcal{D}\frac{\partial^2}{\partial x_j^2}\left(Y^2\psi\right)$. Substitution of the expansion into Eq. 16 yields a final expression for A_ξ,

$$A_\xi = \frac{\partial^2}{\partial \eta^2} \left(Y^2 \psi \mathcal{D} \left(\nabla \xi \right)^2 \right) - \frac{\partial}{\partial \eta} \left(\mathcal{D} \psi \frac{\partial \xi}{\partial x_j} \frac{\partial Y^2}{\partial x_j} \right) - \mathcal{D} \frac{\partial^2}{\partial x_j^2} \left(Y^2 \psi \right) + \mathcal{D} \frac{\partial}{\partial x_j} \left(\psi \frac{\partial Y^2}{\partial x_j} \right) \quad . \tag{17}$$

The particle diffusivity term A_y, as given above in connection with Eq. 15, appears in the full expansion of $\mathcal{D}_y Y \frac{\partial}{\partial x_j}\left(\psi \frac{\partial Y}{\partial x_j}\right)$. Expressing A_y as the subject of this expansion yields

$$A_y = \frac{\partial}{\partial \eta} \left(\mathcal{D}_y \psi \frac{\partial \xi}{\partial x_j} \frac{\partial Y^2}{\partial x_j} \right) + 2 \mathcal{D}_y Y \frac{\partial}{\partial x_j} \left(\psi \frac{\partial Y}{\partial x_j} \right) \quad . \tag{18}$$

Rearrangement of the latter right-hand side term of the above equation via the chain rule gives A_y in final form,

$$A_y = \frac{\partial}{\partial \eta} \left(\mathcal{D}_y \psi \frac{\partial \xi}{\partial x_j} \frac{\partial Y^2}{\partial x_j} \right) + \mathcal{D}_y \frac{\partial}{\partial x_j} \left(\psi \frac{\partial Y^2}{\partial x_j} \right) - 2 \mathcal{D}_y \psi \left(\frac{\partial Y}{\partial x_j} \right)^2 \quad , \tag{19}$$

The substitution of Eqs. 7 and 19 into Eq. 15 yields,

$$\frac{\partial}{\partial t} \left(\psi Y^2 \right) + \frac{\partial}{\partial x_i} \left(u_i \psi Y^2 \right) = 2 \psi Y \dot{\omega} - 2 \mathcal{D}_y \psi \left(\frac{\partial Y}{\partial x_j} \right)^2 + \frac{\partial F_{Y2}}{\partial \eta} + R_{Y2} \quad , \tag{20}$$

where the flux of squared particle mass in mixture fraction space is given by,

$$F_{Y2} = \left(\mathcal{D}_y + \mathcal{D} \right) \psi \frac{\partial \xi}{\partial x_j} \frac{\partial Y^2}{\partial x_j} - \frac{\partial}{\partial \eta} \left(Y^2 \psi \mathcal{D} \left(\nabla \xi \right)^2 \right) \quad , \tag{21}$$

and the collected residual terms can be written as,

$$R_{Y2} = \left(u_i - v_i \right) \psi \frac{\partial Y^2}{\partial x_i} + \left(\mathcal{D}_y - \mathcal{D} \right) \frac{\partial}{\partial x_j} \left(\psi \frac{\partial Y^2}{\partial x_j} \right) + \mathcal{D} \frac{\partial^2}{\partial x_j^2} \left(Y^2 \psi \right) \quad . \tag{22}$$

3.1.2. Averaging and closure of ψY equation

It is illustrative to average and close the simpler equation for conditional mean particle mass fraction before employing the same approach on the conditional variance equation. The conditional mean equation is required before further derivation

of the conditional variance equation can proceed. In this section, some of the key closure assumptions of Klimenko and Bilger (1998) have been relaxed out of necessity for the modeling of particles.

A set of equations similar to Eqs. 20-22 applies for the product of the fine-grain PDF and particle mass fraction and can be written as,

$$\frac{\partial}{\partial t}\left(\psi Y\right) + \frac{\partial}{\partial x_i}\left(u_i \psi Y\right) = \psi\dot{\omega} + \frac{\partial F_Y}{\partial \eta} + R_Y \quad , \tag{23}$$

where

$$F_Y = \left(\mathcal{D}_y + \mathcal{D}\right)\psi\frac{\partial \xi}{\partial x_j}\frac{\partial Y}{\partial x_j} - \frac{\partial}{\partial \eta}\left(Y\psi\mathcal{D}\left(\nabla\xi\right)^2\right) \quad , \tag{24}$$

and

$$R_Y = \left(u_i - v_i\right)\psi\frac{\partial Y}{\partial x_i} + \left(\mathcal{D}_y - \mathcal{D}\right)\frac{\partial}{\partial x_j}\left(\psi\frac{\partial Y}{\partial x_j}\right) + \mathcal{D}\frac{\partial^2}{\partial x_j^2}\left(Y\psi\right) \quad . \tag{25}$$

Averaging Eq. 23 over mixture fraction space yields the PDF-product form of the conditional moment closure (CMC) equation for conditional mean particle mass fraction,

$$\frac{\partial}{\partial t}\left(P_\eta Q_\eta\right) + \frac{\partial}{\partial x_i}\left(\left\langle u_i Y \mid \eta\right\rangle P_\eta\right) = \left\langle\dot{\omega} \mid \eta\right\rangle P_\eta + \frac{\partial F_Q}{\partial \eta} + R_Q \quad , \tag{26}$$

where $Q_\eta \equiv \left\langle Y \mid \eta\right\rangle = \left\langle Y\psi\right\rangle / P_\eta$, and F_Q and R_Q are the conditionally averaged flux and residual terms. The averaged residual term can be written as follows,

$$R_Q = \left\langle\left(u_i - v_i\right)\frac{\partial Y}{\partial x_i} \mid \eta\right\rangle P_\eta + \left(\mathcal{D}_y - \mathcal{D}\right)\frac{\partial}{\partial x_j}\left(P_\eta\left\langle\frac{\partial Y}{\partial x_j} \mid \eta\right\rangle\right) + \mathcal{D}\frac{\partial^2}{\partial x_j^2}\left(QP_\eta\right) \quad , \tag{27}$$

and contains terms which are assumed to be small for high Reynolds number flow with only small particle slip velocities. The conditional mean flux term, equal to

$$F_Q = \left(\mathcal{D}_y + \mathcal{D}\right)P_\eta\left\langle\frac{\partial \xi}{\partial x_j}\frac{\partial Y}{\partial x_j} \mid \eta\right\rangle - \frac{\partial}{\partial \eta}\left(\mathcal{D}P_\eta\left\langle Y\left(\nabla\xi\right)^2 \mid \eta\right\rangle\right) \quad , \tag{28}$$

is approximated by Klimenko and Bilger (1998) after assuming that the gradient of Y is well correlated with the gradient of mixture fraction and that there is only a weak correlation between Y and $\left(\nabla\xi\right)^2$. In the following, the latter assumption is relaxed, so that

$$F_Q \approx c\, P_\eta N_\eta\frac{\partial Q_\eta}{\partial \eta} - Q_\eta\frac{\partial}{\partial \eta}\left(P_\eta N_\eta\right) - \frac{\partial}{\partial \eta}\left(P_\eta C_\eta\right) \quad , \tag{29}$$

where $N_\eta \equiv \left\langle\mathcal{D}\left(\nabla\xi\right)^2 \mid \eta\right\rangle$ is the scalar dissipation rate and C_η is the covariance between scalar dissipation rate and particle mass fraction. The symbol c denotes a *mixing mode* variable which is equal to unity in the case of mixing in the absence of

differential diffusion but is not known for the case of differentially diffusing scalars (Klimenko & Bilger 1998). This variable is discussed in greater detail in Section 3.2.

The final form of the equation for conditional mean particle mass fraction is obtained by substituting Eq. 29 into Eq. 26, followed by subtraction of the mixture fraction PDF equation (averaged form of Eq. 14) and normalization by the PDF to give,

$$\frac{\partial Q_\eta}{\partial t} + \langle u_i \mid \eta \rangle \frac{\partial Q_\eta}{\partial x_i} = \langle \dot{\omega} \mid \eta \rangle + cN_\eta \frac{\partial^2 Q_\eta}{\partial \eta^2} + (c-1) M_\eta \frac{\partial Q_\eta}{\partial \eta} - \frac{1}{P_\eta} \frac{\partial^2}{\partial \eta^2} \left(P_\eta C_\eta \right) \quad . \tag{30}$$

In the above expression, R_Q has been neglected as has the conditional correlation between velocity fluctuations and particle mass fraction. As in Eq. 7, the symbol M_η denotes the conditional mean diffusion rate.

3.1.3. Averaging and closure of ψY^2 equation

The equation for the conditional variance of particle mass fraction, defined as $q_\eta^2 \equiv \langle y^2 \mid \eta \rangle = \langle Y^2 \psi \rangle / P_\eta - Q_\eta^2$, can be derived from Eq. 20 through several stages. Averaging of Eq. 20 yields a mean-square-PDF product equation,

$$\frac{\partial}{\partial t} \left(P_\eta \langle Y^2 \mid \eta \rangle \right) + \frac{\partial}{\partial x_i} \left(\langle u_i Y^2 \mid \eta \rangle P_\eta \right) = 2 \langle Y \dot{\omega} \mid \eta \rangle P_\eta + \frac{\partial F_q}{\partial \eta} - P_\eta \epsilon_Y + R_q \quad , \tag{31}$$

where F_q denotes the flux of mean square mass in mixture fraction space, R_q is the average of the Y^2 residual term of Eq. 22,

$$R_q = P_\eta \left\langle (u_i - v_i) \frac{\partial Y^2}{\partial x_i} \mid \eta \right\rangle + (\mathcal{D}_y - \mathcal{D}) \frac{\partial}{\partial x_j} \left(P_\eta \left\langle \frac{\partial Y^2}{\partial x_j} \mid \eta \right\rangle \right) + \mathcal{D} \frac{\partial^2}{\partial x_j^2} \left(P_\eta \langle Y^2 \mid \eta \rangle \right) \quad , \tag{32}$$

and ϵ_Y is the conditional mean square mass dissipation rate, given by

$$\epsilon_Y \equiv 2\mathcal{D}_y \left\langle (\nabla Y)^2 \mid \eta \right\rangle \quad . \tag{33}$$

Following the closure argument for flux of conditional mean mass in mixture fraction space (Eq. 29), the flux of the conditional mean square particle mass fraction,

$$F_q = (\mathcal{D}_y + \mathcal{D}) P_\eta \left\langle \frac{\partial \xi}{\partial x_j} \frac{\partial Y^2}{\partial x_j} \mid \eta \right\rangle - \frac{\partial}{\partial \eta} \left(P_\eta \left\langle Y^2 \mathcal{D} (\nabla \xi)^2 \mid \eta \right\rangle \right) \quad , \tag{34}$$

is approximated by the following, where the mixing mode variable c has a value equal to that employed in Eq. 29,

$$F_q \approx c\, P_\eta N_\eta \frac{\partial q_\eta^2}{\partial \eta} - q_\eta^2 \frac{\partial}{\partial \eta} \left(P_\eta N_\eta \right) + 2c\, P_\eta C_\eta \frac{\partial Q_\eta}{\partial \eta} - 2 Q_\eta \frac{\partial}{\partial \eta} \left(P_\eta C_\eta \right)$$

$$+ c P_\eta N_\eta \frac{\partial Q_\eta^2}{\partial \eta} - Q_\eta^2 \frac{\partial}{\partial \eta} \left(P_\eta N_\eta \right) \quad . \tag{35}$$

Following the substitution of Eq. 35 into Eq. 31, the decomposition of Y into $Q_\eta + y$, and the subtraction of the equation for the conditional mean mass fraction, the equation for the product of conditional variance and mixture fraction PDF is derived. The decomposition of this equation via the chain rule and subtraction of the PDF equation multiplied by q_η^2 yields the final form of the conditional variance equation,

$$\frac{\partial q_\eta^2}{\partial t} + \langle u_i \mid \eta \rangle \frac{\partial q_\eta^2}{\partial x_i} = 2 \langle y \dot{\omega}' \mid \eta \rangle + c N_\eta \frac{\partial^2 q_\eta^2}{\partial \eta^2} + (c-1) M_\eta \frac{\partial q_\eta^2}{\partial \eta} + S_q - \epsilon_q \quad , \tag{36}$$

where S_q denotes the collected conditional source terms for particle mass fraction variance,

$$S_q \equiv 2 c C_\eta \frac{\partial^2 Q_\eta}{\partial \eta^2} + \frac{2}{P_\eta} (c-1) \frac{\partial}{\partial \eta} (P_\eta C_\eta) \frac{\partial Q_\eta}{\partial \eta} + 2 \left(c - \frac{\mathcal{D}_y}{\mathcal{D}} \right) N_\eta \left(\frac{\partial Q_\eta}{\partial \eta} \right)^2 \quad , \tag{37}$$

and ϵ_q is the dissipation rate of conditional variance,

$$\epsilon_q \equiv 2 \mathcal{D}_y \left\langle (\nabla y)^2 \mid \eta \right\rangle \quad . \tag{38}$$

Note that the conditional variance equation in the form given above neglects conditional covariance between velocity and mass fraction and all of the terms associated with the difference between R_q and $2 Q_\eta R_Q$ which appear in the derivation.

The final forms of the equations for the conditional mean and variance of particle mass fraction (Eqs. 30 and 36) contain two unclosed quantities, namely the mixing mode variable c, which parameterizes the level of differential diffusion, and the covariance between scalar dissipation rate and particle mass fraction C_η. A discussion of these two quantities is provided in the following sections.

3.2 Solution of model equations

Equations 30 and 36 of the preceding section were solved to match the simulated conditions of spatially homogeneous, steady conditional statistics. The statistically stationary, spatially degenerate form of the conditional mean particle mass fraction profile is given by,

$$0 = \langle \dot{\omega} \mid \eta \rangle + c N_\eta \frac{\partial^2 Q_\eta}{\partial \eta^2} + (c-1) M_\eta \frac{\partial Q_\eta}{\partial \eta} - \frac{1}{P_\eta} \frac{\partial^2}{\partial \eta^2} (P_\eta C_\eta) + I_Q \quad , \tag{39}$$

where I_Q is the conditional mean particle mass injection rate which results from the injection process described in Section 2.1. The conditional variance of particle mass fraction profile was found from,

$$0 = 2 \langle y \dot{\omega}' \mid \eta \rangle + c N_\eta \frac{\partial^2 q_\eta^2}{\partial \eta^2} + (c-1) M_\eta \frac{\partial q_\eta^2}{\partial \eta} + S_q + I_q \quad , \tag{40}$$

where I_q is the conditional variance source due to particle injection. Note that the effective diffusivity of the particle field ($\mathcal{D}_y$) was assumed to be identically zero, thus the absence of the ϵ_q term given in Eq. 36 from the above equation. The conditional particle injection source terms included in the above (I_Q & I_q) are given by,

$$I_Q = \frac{P_I}{\tau_{pop}} \left(1 - Q_\eta\right) \tag{41}$$

$$I_q = \frac{P_I}{\tau_{pop}} \left(\left(1 - Q_\eta\right)^2 - q_\eta^2\right) \tag{42}$$

where P_I is the PDF of particle injection mixture fraction and τ_{pop} is the time required for the number of injections to equal the size of the particle population. In the above it was assumed that particles were injected to replace those which leave the system, and all freshly injected particles had unit mass as described in Section 2.1. The form of the injection PDF consisted of the normalized sum of two Gaussian distributions with variances equal to the domain variance and mean mixture fraction values of zero and unity.

Chemical source terms in Eqs. 39 and 40 were determined using instantaneous local temperature (taken from an invariant chemical equilibrium profile) and the conditional mean and variance of particle mass fraction in truncated Taylor series expansions of the instantaneous reaction rate expressions.

The *mixing mode* variable c, included in the CMC equations above, provides a means of accounting for differential diffusion effects. In the limit where mixing is overwhelmingly due to turbulent stirring, the mixing mode variable tends to unity. In cases where a larger proportion of the mixing is due to molecular mass transfer, the mixing mode variable will vary substantially from unity. The greatest allowable deviation of c from unity is given by the ratio of the molecular diffusivity of the species in question to that of the mixture fraction.

From a modeler's perspective, it is highly desirable that c be independent of Q_η, q_η^2, and mixture fraction. In that eventuality, one could hypothesize that the degree of departure from mixing that is dominated by strong turbulent stirring might be expressed as,

$$c = 1 + \left(\frac{\mathcal{D}_y}{\mathcal{D}} - 1\right) f_{mix} \quad , \tag{43}$$

where f_{mix} is a function which varies between zero and unity according to some dependence on global properties of the flow field. One possibility for f_{mix} is some power of the Kolmogorov scalar scale ξ_k appropriately normalized by the maximum globally realizable range in mixture fraction. The Kolmogorov scalar scale is a measure of the characteristic size of scalar fluctuations at dissipative scales. For mixture fraction this scale varies between zero and unity for high and low intensity turbulent mixing respectively. As this study consists of data from a single set of mixing conditions, it is not possible to validate any model for variation in c with mixing conditions. It is, however, possible to examine whether a single value of c

is appropriate independently of local values of Q_η, q_η^2, and mixture fraction. This issue is examined in the next section.

It should be noted that Kronenburg and Bilger (1997) successfully account for differential diffusion in the CMC model through the use of an alternate treatment to that proposed above. Their methodology has much to recommend it, but when applied to multi-component reacting systems, it requires an additional conditional moment equation to be solved for each species. The method presented here seeks to avoid that added cost.

It was found that the profile shape and magnitude of the conditional covariance between particle mass fraction and scalar dissipation rate (C_η) was critical to the transport of particles in mixture fraction space. While the form of this profile is, in general, not known, its behavior at mixture fraction bounds is prescribed by the integration of Eq. 26, with respect to mixture fraction, between these bounds. This integration should yield the unconditional mean mixture fraction equation, which implies that the bounding values of the mixture fraction flux term (Eq. 29) are zero. It follows that the slope of the product $P_\eta C_\eta$ must be zero at the bounding mixture fractions.

Modeling of the C_η term was achieved using a simple heuristic approach to best match the observed simulation profiles for C_η. This model took the form,

$$C_\eta = \left(a_q \sqrt{(q_\eta^2)} - a_Q Q_\eta + a_{cor} \right) N_\eta \quad , \tag{44}$$

where a_q, a_Q, and a_{cor} were constants determined from the goodness of fit with the C_η profile observed from the corresponding simulation. The above fitting technique is similar to that employed by Li and Bilger (1996) except for the inclusion of the conditional mean value (Q_η) and the zero-boundary correction term a_{cor}. It was found that it was necessary to include these terms to match the observed simulation data. Due to the case-specific nature of the covariance profiles, they are discussed in turn in the following section.

4. Results

In the following, the results from the modeling of soot particles and droplets are discussed separately.

4.1 Soot

Examining the conditional covariance between scalar dissipation rate and particle mass fraction (C_η), the simulation data revealed the characteristic form of the covariance profile for soot as possessing a large negative spike near the mean mixture fraction. The location of this spike in mixture fraction space corresponded with the location of the peak conditional mean mass fraction. Through careful selection of the coefficients in the C_η model equation (Eq. 44), it was possible to produce the similar profile as was observed in the simulation data while producing good predictions for Q_η and q_η^2.

The profile match derived for conditional covariance in soot case *s1* can be seen in Fig. 2. Note that the observed simulation profile has been slightly smoothed

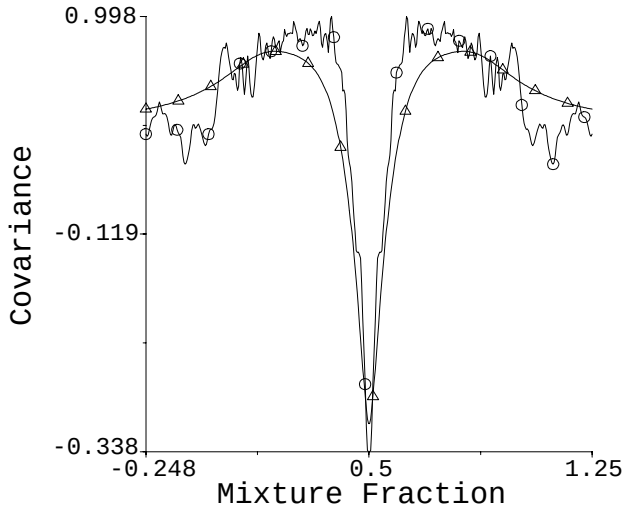

FIGURE 2. Modeled and observed conditional covariance between mass fraction and scalar dissipation rate for case *s1*. Symbols denote the following profiles: △ - prediction of covariance, and ○ - simulated covariance.

and averaged about the symmetry point at the mean mixture fraction to facilitate comparison with the smooth symmetric model profile. It is evident that the model profile agrees reasonably well with the observed profile, particularly in the vicinity of the mean mixture fraction. The model profile does not match the observed maximum value of the covariance at mixture fractions slightly leaner and richer than the mean value. Unfortunately, it is the first and second derivatives of the conditional covariance which appear in the model equations. The value of the slope and curvature of the model C_η profile are believed to reflect the general behavior of the simulation data; however, it is difficult to make any stronger statement due to the limited data available for statistical analysis. Future simulations with larger particle populations will be used to better understand this behavior.

The characteristic effect on the conditional mean particle mass fraction of varying the mixing mode variable, c, can be seen in Fig. 3 for case *s1* along with the conditional mean profile which results from chemical reactions and particle injection alone. It can be seen that the arbitrary increase of c causes the predicted mean mass fraction profile to simultaneously increase in peak value and decrease in minimum value. Further, increases in c tend to decrease the value of conditional mean mass fraction at very rich and very lean mixture fractions.

The governing conditional mean particle mass fraction equation (Eq. 39) has the property that increased values of c tend to favor a mode of mass transfer *in mixture fraction space* which is essentially diffusive in nature. Lower values of c favor the mode associated with the drift of particle mass *in mixture fraction space* which results from gas phase species diffusing at a more rapid rate in physical space than the particles they surround. Thus c can be thought of as a measure of to what degree particle mass diffuses against a mixture fraction coordinate instead of undergoing an apparent convection-like process in mixture fraction space due to the differential

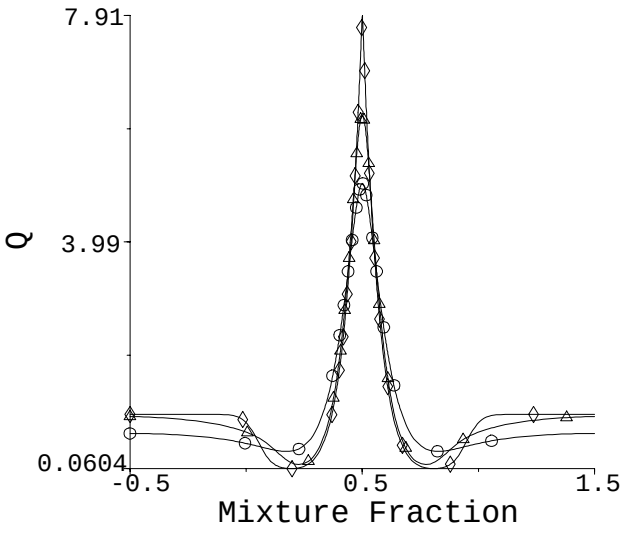

FIGURE 3. Predicted conditional mean mass fraction profiles for case *s1* with arbitrarily varied levels of differential diffusion. Symbols denote the following profiles: △ - prediction with $c = 0.05$, ○ - prediction with $c = 1.00$, and ◇ - chemical equilibrium with particle injection.

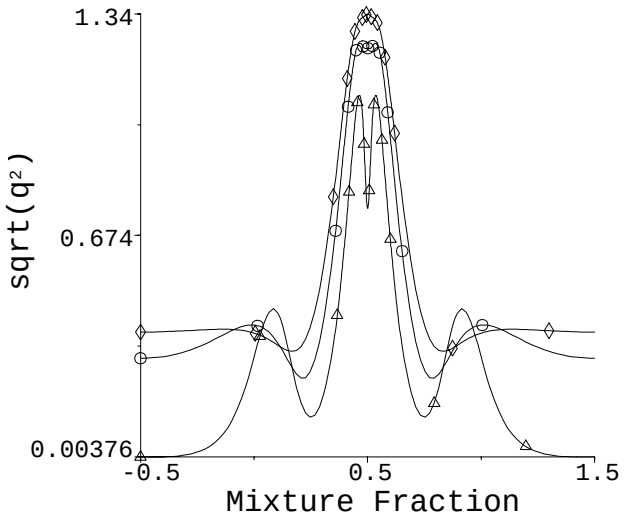

FIGURE 4. Predicted conditional root mean square deviation ($\sqrt{(q_\eta^2)}$) mass fraction profiles for case *s1* with arbitrarily varied levels of differential diffusion. Symbols denote the following profiles: △ - prediction with $c = 0.05$, ○ - prediction with $c = 0.50$, and ◇ - prediction with $c = 1.00$.

diffusion of the coordinate and mass fraction fields in physical space. The tendency towards smoother conditional mean profiles, in Fig. 3, with increased c values is indicative of this trend.

Variation in the predicted conditional mass fraction variance profiles with arbitrary variation in the mixing mode variable can be seen in Fig. 4 for case *s1*. It is apparent that increasing the value of c leads to an increased peak value in the

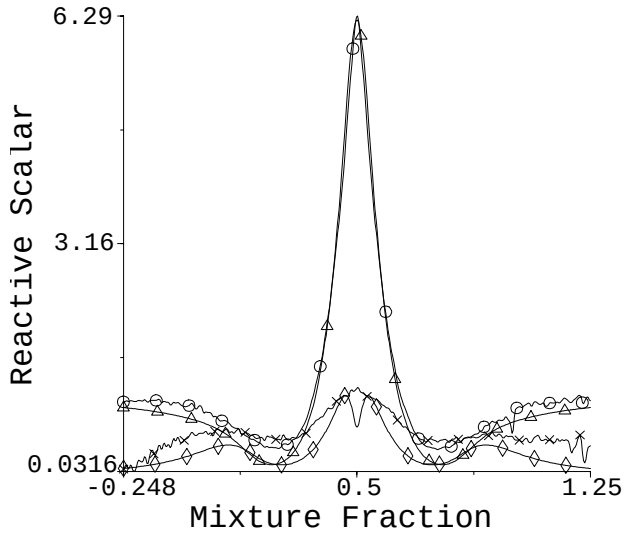

FIGURE 5. Modeled and observed conditional mean and variance of particle mass fraction for case *s1*. Symbols denote the following profiles: $\triangle$ - Q_η prediction, $\circ$ - simulated Q_η, $\diamond$ - q_η prediction, and $\times$ - simulated q_η.

conditional mean variance profiles and an increased value of variance at very rich and lean mixture fractions. The elevated level of conditional variance in the high c case is due to the source contribution from the last term of S_q (see Eq. 37).

A low value of c results in a dip in variance near the mean mixture fraction where the model equations do not predict any variance production. This dip is not present in higher c cases where diffusive transport in mixture fraction space is strong enough to smooth out sharp changes in gradient.

The result of matching the conditional covariance profile and minimizing the mixing mode variable to $c = 0.05$ (minimum numerically stable value) provided the predicted conditional mean and variance profiles plotted in Fig. 5.

Employing the same value of c and the same constants in the model for the mass-dissipation covariance C_η from Eq. 44 provided accurate predictions for the conditional mean and variance of particle mass in soot case *s2i*. These predictions are plotted against simulation data in Fig. 6.

It is evident that there is reasonable qualitative agreement between the predicted and observed profiles in Figs. 5 and 6. The CMC model captures the essential changes in profile shape in the more reactive case (Fig. 5) but appears to incorrectly predict rich and lean side behavior to greater extent in the less reactive case. Good quantitative agreement is found near the mean mixture fraction in both cases; however, the predicted profiles deviate substantially from the observed data at mixture fractions away from the mean. This discrepancy may have been due to the poor modeling of the conditional covariance term (C_η) at those same mixture fractions. It is difficult to be sure that the model fit to C_η provided by Eq. 44 provides accurate C_η gradients and curvatures as is required in the CMC equations. It is clear that the modeling of the mass-dissipation covariance requires further attention.

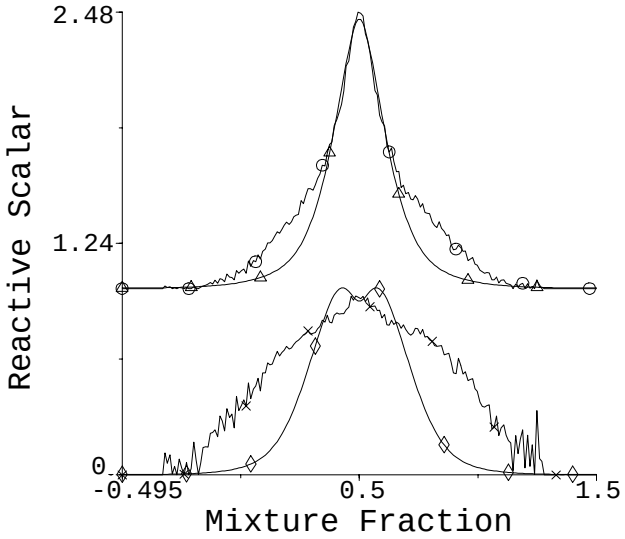

FIGURE 6. Modeled and observed conditional mean and variance of particle mass fraction for case *s2*. Symbols denote the following profiles: $\triangle$ - Q_η prediction, $\circ$ - simulated Q_η, $\diamond$ - q_η prediction, and $\times$ - simulated q_η.

4.1.1 Effect of particle slip velocity

Soot cases *s2* and *s2i* were simulated to examine the effect of slip velocities between particles and their carrier fluid. The former simulated case took account of particle inertia and the difference in local velocities which can arise from the kinetic lag between fluid flow variations and particle response to those variations. The latter simulation case (*s2i*) did not account for particle inertia and thus no slip velocities were present.

The differences in the conditional mean and variance particle mass fraction profiles between these two simulation cases can be seen in Fig. 7. It is evident that the introduction of particle inertia, all else being equal, causes the conditional mean particle field to behave in a more diffusive manner in mixture fraction space. Simultaneously, a rise in conditional variance results, particularly at mixture fractions away from the mean mixture fraction. Although not plotted, there appeared to be little change in the C_η profiles between the simulation pair, indicating that the vee-shaped form of the covariance profile is not a result of inertial particle transport.

Conditional source terms related to particle slip velocity appear in the neglected residual groupings of Eqs. 39 and 40. The conditional mean equation contains the slip transport term $\langle (u_i - v_i) \mid \eta \rangle \frac{\partial}{\partial \eta} (Q_\eta)$, whereas the variance equation contains a transport term $\langle (u_i' - v_i') \mid \eta \rangle \frac{\partial}{\partial \eta} \left(q_\eta^2 \right)$, and the source term $\langle (u_i' - v_i')\, y \mid \eta \rangle \frac{\partial}{\partial \eta} (Q_\eta)$. The difference in behavior observed in the above simulation cases corresponds with the expected effect of the neglected slip velocity terms in the CMC equations. It is clear that the introduction of larger inertial particles to the model problem gives rise to a significant increase in the difficulty of modeling particle behavior.

4.2 Droplets

Unlike the soot particles, the droplet particle simulations exhibited very weak

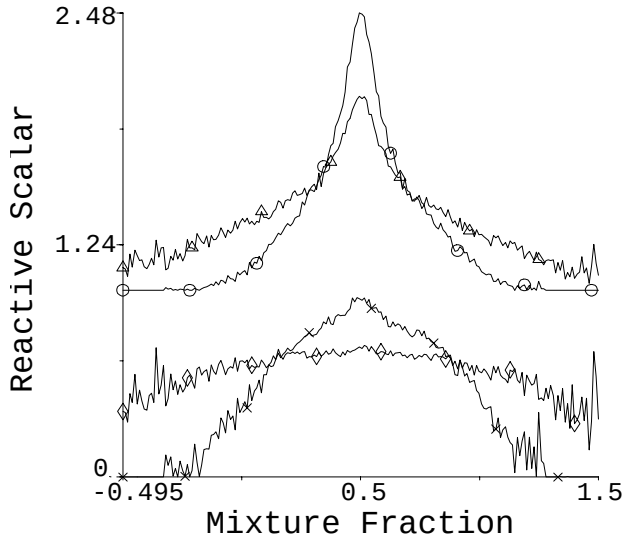

FIGURE 7. Observed conditional mean and variance of particle mass fraction for inertial (*s2*) and inertia-less (*s2i*) soot cases. Symbols denote the following profiles: $\triangle$ - Q_η inertial, $\circ$ - Q_η inertia-less, $\diamond$ - q_η inertial, and $\times$ - q_η inertia-less.

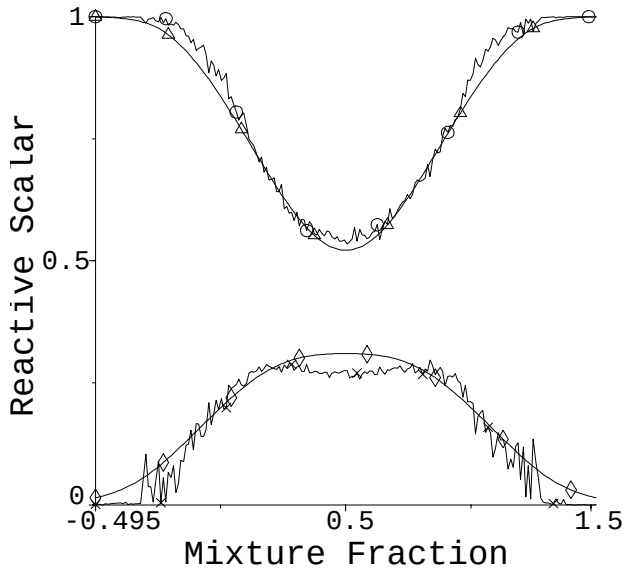

FIGURE 8. Modeled and observed conditional mean and variance of particle mass fraction for case *d1i*. Symbols denote the following profiles: $\triangle$ - Q_η prediction, $\circ$ - simulated Q_η, $\diamond$ - q_η prediction, and $\times$ - simulated q_η.

conditional covariance between scalar dissipation rate and particle mass fraction. This distinction between the particle types suggests that the form of the covariance (C_η) profile is linked to the types of reactions which act upon the particles. It would seem that strong reactions, as in the soot cases, give rise to sharp changes in particle properties in mixture fraction space which in turn impact strongly upon the transport statistics between adjacent mixture fractions. The weak reactions of

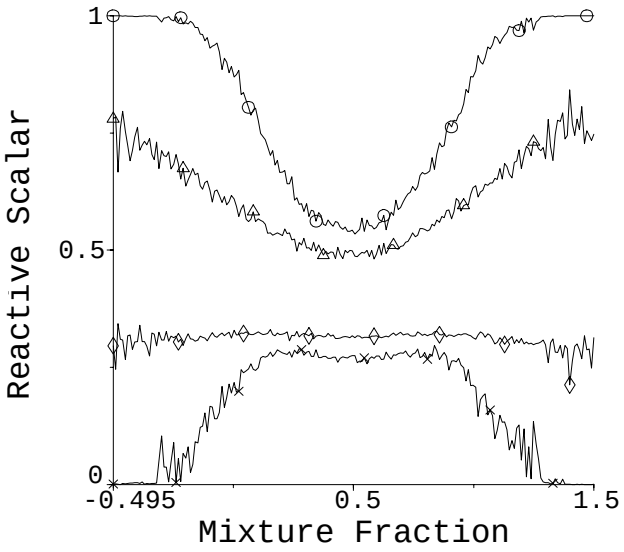

FIGURE 9. Observed conditional mean and variance of particle mass fraction for inertial (*d1*) and inertia-less (*d1i*) droplet cases. Symbols denote the following profiles: $\triangle$ - Q_η inertial, $\circ$ - Q_η inertia-less, $\diamond$ - q_η inertial, and $\times$ - q_η inertia-less.

the droplet cases do not impart sharp changes in value to the conditional statistical profiles and thus do not seem to cause strong covariance between mass fraction and scalar dissipation rate. Further investigation of this behavior is clearly warranted.

Due to the observed behavior in the droplet cases, the covariance profile was modeled as being zero for all mixture fractions. As with the soot cases, the value of the mixing mode parameter, which gave best predicted agreement with the observed mass fraction profiles, was very low ($c = 0.1$). The degree of agreement between the observed and predicted profiles for the inertia-less droplet case (*d1i*) can be inferred from Fig. 8. It is clear that the CMC model predicts the conditional mean and variance of droplet mass fraction with a good degree of accuracy.

4.2.1 Effect of particle slip velocity

While it is clear that the CMC model can capture the behavior of very small fuel droplets in the terminal stage of evaporation, the modeling of particles with significant inertia is more problematic.

In Fig. 9, the conditional statistics from the simulation pair of *d1* and *d1i* are compared. It is evident that, as with the soot comparison of Fig. 7, the larger inertial particles tend to exhibit a tendency towards conditional mean profiles which have a lower level of curvature as though smoothed by enhanced diffusive transport. The conditional variance profile exhibits virtually no change in slope in the case of the inertial particles. The existence of slip velocities, larger than in the inertial soot case, causes a great deal of conditional variance generation to occur at mixture fractions away from the mean.

The noted inertial-particle behavior is even stronger in nature than that described in Section 4.1.1 for smaller soot particles. This suggests that the larger the particles

under consideration, the less effective a continuum model will be in describing their behavior.

5. Remarks

The results of this preliminary study indicate that a tailored variant of the Conditional Moment Closure (CMC) method can be applied successfully to modeling the evolution of soot-like and droplet-like reacting particles in a turbulent combusting environment. For the soot particle cases, a single set of constants were sufficient to correctly predict particle evolution under for a variety of reaction intensities. This finding suggests that it is appropriate to simultaneously model condensed and gas phase reactions in turbulence using the CMC model within an Eulerian frame.

However, significant caveats apply to this modeling approach. Firstly, it is clear that the conditional covariance between scalar dissipation rate and reactive scalar mass fraction cannot, in general, be neglected. It is apparent that some species can exhibit strong non-zero covariance profiles which play the foremost role, of all transport terms, in transporting scalar properties in mixture fraction space. An examination of simulation cases with different particle reactivities suggest that those species subject to more intense reactions exhibit stronger covariance profiles. This may be due to the establishment of large changes in scalar values and gradients between adjacent mixture fractions, which can result from strong reactions taking place. It was found that changes in particle inertia, while keeping all else constant, had virtually no effect on the form of the conditional covariance profile. Further work is obviously required to study the dependence of mixing covariance on particle reactivity and to devise an improved model for predicting its profile shape in mixture fraction space.

Secondly, it was found that the CMC model is not well suited to predicting the behavior of particles with substantial levels of inertia. Relatively large particles such as fuel droplets can develop significant slip velocities relative to their surrounding fluid. These slip velocities appear as unclosed transport and variance production terms in the CMC equations. They appear to enhance transport of particle properties in mixture fraction space over that exhibited by smaller particles with smaller slip velocities but similar reactivity. Further, as one would expect, because the larger particles are not transferred in space in the same way as gaseous mixture fraction, the conditional variance of particle properties at any given mixture fraction is higher than that for gaseous species. While it was found that the modeling of inertial particle transport in mixture fraction space could largely be accounted for by increasing the level of diffusive transport (through increasing c to unrealistically high levels), the model could not account for the increased conditional variance which was observed.

The mixing mode variable (c) approach to treating differential diffusion in the CMC model deserves further attention. In varying the value of c between the extreme value given by the ratio of molecular diffusivities and unity, according to changes in global mixing conditions, the CMC equations change in a natural way to embody differential diffusion effects to a greater or lesser degree as required.

A single value of c was found to suffice for the prediction of particle behavior in the cases studied here under uniform mixing conditions, but with widely different reactive behavior. This suggests c may well be independent of local variations in mixture fraction and particle mass fraction and a function only of global mixing parameters. Further work is required to properly test this hypothesis and the model for c proposed in Eq. 43.

Future work involving the CMC-particle model derived here will focus on validation of the model against larger simulations which incorporate more realistic chemistry, higher turbulence levels, and a more diverse set of mixing and reaction conditions.

REFERENCES

Bilger, R. W. 1993 Conditional Moment Methods for Turbulent Reacting Flow. *Phys. Fluids.* **5,** 436-444.

Klimenko, A. Yu. 1990 Multicomponent Diffusion of Various Admixtures in Turbulent Flow. *Fluid Dyn.* **25,** 327-334.

Klimenko, A. Yu., Bilger, R. W. 1998 Conditional Moment Closure for Turbulent Combustion. Submitted to *Progress in Energy and Combustion Science.*

Kronenburg, A., & Bilger, R. W. 1997 Modeling of Differential Diffusion Effects in Nonpremixed Nonreacting Turbulent Flow. *Phys. Fluids.* **9,** 1435-1447.

Kuo, K. K., *Principles of Combustion*, John Wiley and Sons, New York. 1986.

Li, J. D., & Bilger, R. W. 1996 The diffusion of conserved and reactive scalars behind line sources in homogeneous turbulence. *J. Fluid Mech.* **8,** 339-372.

Overholt, M. R., & Pope, S. B. 1996 Direct numerical simulation of a passive scalar with an imposed mean gradient in isotropic turbulence. *Phys. Fluids.* **8,** 3128-3148.

Pope, S. B. 1985 PDF Methods for Turbulent Flows. *Progress in Energy and Comb. Sci.* **11,** 119-192.

Pope, S. B., & Ching, E. S. C. 1993 Stationary probability density functions: An exact result. *Phys. Fluids.* **5,** 1529.

Yeung, P. K., & Pope, S. B. 1988 An Algorithm for Tracking Fluid Particles in Numerical Simulations of Homogeneous Turbulence. *J. Comp. Phys.* **79,** 373-416.

Yeung, P. K., & Pope, S. B. 1989 Measurements of particle dispersion obtained from direct numerical simulation of isotropic turbulence. *J. Fluid Mech.* **207,** 531-586.